Materials Chemistry and Physics 301 (2023) 127685

Contents lists available at ScienceDirect

Materials Chemistry and Physics

journal homepage: www.elsevier.com/locate/matchemphys

Radiative recombination pathways in ordered and disordered CZTSe microcrystals

İ. Mengü *, J. Krustok, R. Kaupmees, V. Mikli, M. Kauk-Kuusik, M. Grossberg-Kuusk

Department of Materials and Environmental Technology, Tallinn University of Technology, Ehitajate tee 5, 19086, Tallinn, Estonia

HIGHLIGHTS

- Photoluminescence study of CZTSe microcrystals with different degrees of disorder is presented.
- The emission bands were located at 0.88 and 0.92 eV at T = 10 K for disordered and ordered samples, respectively.
- Localized electron states were detected in both samples, being deeper in the ordered CZTSe.
- The PL bands were attributed to TI and BI transitions coexisting at low temperatures.

ARTICLE INFO

Keywords:
$Cu_2ZnSnSe_4$
Order-disorder
Photoluminescence
Raman spectroscopy

ABSTRACT

The photoluminescence (PL) spectra of $Cu_2ZnSnSe_4$ microcrystals with two different degrees of disorder were investigated by measuring the dependencies on the temperature and excitation power. Crystals were cooled at different rates after the high-temperature annealing treatment in order to change the degree of disorder. The PL spectra of both samples consist of one asymmetrical band located at 0.88 and 0.92 eV for disordered and ordered crystals, respectively. At low temperatures, both samples have similar origins of PL involving localized electron states. In the case of the ordered sample, we observed deeper localized electron states, thus higher temperatures were needed to empty the electrons from these states to the band states. Changes in the degree of disorder lead to changes in the radiative recombination in CZTSe microcrystals.

1. Introduction

$Cu_2ZnSnSe_4$ (CZTSe) is a p-type semiconductor having a kesterite crystal structure and optimal properties for solar energy conversion, which have drawn considerable research attention to it as the absorber layer for thin film photovoltaics [1,2]. A power conversion efficiency of 12.5% has been achieved with a CZTSe thin film solar cell [3]. CZTSe-based solar cell device efficiency is still limited by severe charge carrier recombination losses caused by bulk defects as well as interface defects due to non-optimal interfaces in the device structure. Due to the quaternary nature of the CZTSe, the concentration of intrinsic point defects is in most cases quite high causing a widening of the defect levels within the band gap, producing spatial electrostatic potential fluctuations and the formation of band tails [4]. Moreover, in multinary compounds, compositional fluctuations can also give rise to disorder and cause additional fluctuations in the bandgap energy [5]. Therefore, the key to higher device efficiencies is knowledge and control over the defect structure of CZTSe.

One of the methods to study radiative recombination and related defects in semiconductors is photoluminescence (PL) spectroscopy. The low-temperature PL emission of CZTSe usually consists of a wide asymmetric band having a peak position at about 0.93 eV [6–11] and involves either a deep acceptor defect or localized deep valence band tail states in the related recombination process. However, it should be mentioned that in some cases very narrow bands can be seen in the low-temperature PL spectra of CZTSe, suggesting the possibility that in the absence of potential fluctuations, recombination is possible through very shallow defect levels or even due to exciton emission [12,13]. The radiative recombination in kesterites can mainly arise from three different channels: band-to-tail (BT) involving a free electron and a hole that is localized in the valence band tail; band-to-impurity (BI) involving a free electron and a hole localized at deeper acceptor defects, which do not overlap with the valence band tail, band-to-band (BB) involving a free electron and a free hole [6]. However, in strongly compensated

* Corresponding author.
E-mail address: idil.mengu@taltech.ee (İ. Mengü).

https://doi.org/10.1016/j.matchemphys.2023.127685
Received 7 December 2022; Received in revised form 22 March 2023; Accepted 27 March 2023
Available online 28 March 2023

semiconductors, potential wells can localize holes and also electrons, thus tail-to-impurity (TI) and tail-to-tail (TT) recombinations are possible [14].

It is assumed that in p-type semiconductors, electrons have considerably lower effective mass, whereby the heavy-doping condition is much more readily satisfied for donors than for acceptors [15]. In that case, an electron does not form a bound state at a single donor and the deep potential wells for electrons can be formed by a high concentration of donor defects [14] or by specific neutral defect clusters [16]. In compensated semiconductors, donor and acceptor concentration values approach each other due to a reduction of the density of free charge carriers [15]. These potential wells appear in strongly compensated seminconductors as a result of a deep modulation of electron density. Also, the level of compensation is the main determinant for the length of the density of states tails in a semiconductor. As a result, in semiconductors with high levels of doping and compensation, radiative transitions occur via neighbouring impurity aggregates (defect clusters) and not isolated impurities [17,18].

Compared to the individual defects, the formation energy of defect clusters in kesterites is lower and among them, $(2Cu_{Zn}^{-}+Sn_{Zn}^{2+})$ has the lowest formation energy [16]; thus, it is predicted, that the concentration of this cluster is relatively high. In the case of many clusters, the valence and conduction band edges show local shifts and both electrons and holes can localize in these potential wells causing TT or TI recombination [19]. Grossberg *et al.* detected a local band gap decrease of 0.35 eV in near-stoichiometric Cu_2ZnSnS_4 (CZTS) polycrystals originating from $(2Cu_{Zn}^{-}+Sn_{Zn}^{2+})$ clusters and enabling recombination of electrons and holes localized in this so-called 3D quantum well [20]. However, localized electron states and TT as well as TI recombinations in CZTSe were not completely understood and more studies are required. Localized states for electrons were studied using PL spectroscopy in various materials including kesterites, chalcopyrites and quantum wells [15,21–25]. In all cases, the materials present wide and asymmetric PL band and the characteristic behavior in PL peak position with increasing temperature. However, TI and TT recombinations were not observed in CZTSe before.

The peak position of the asymmetric PL band and the bandgap energy (E_g) of CZTSe depend also on the disorder between Cu and Zn in the Cu/Zn planes leading to the formation of Zn_{Cu}^{+} and Cu_{Zn}^{-} antisite defects [26,27]. In ordered CZTSe, the room temperature bandgap energy is about 100 meV higher than in disordered one, being 1.05 and 0.95 eV for Ord-CZTSe and Dis-CZTSe, respectively [26]. Mainly, Cu-Zn disorder appears due to the same effective cation radius of Cu^{1+} and Zn^{2+} ions in the lattice. This causes a facile exchange between Cu and Zn atoms which overall results in an energetically more favorable state of the system [28]. This also explains the low formation energy (0.21 eV) of the Cu-Zn antisite pair $(Cu_{Zn}^{-}+Zn_{Cu}^{+})$ [29]. The formation of this defect pair undergoes a second-order phase transition at around a critical temperature of 200 °C for CZTSe [27]. Above this critical temperature, CZTSe crystals demonstrate a complete cation disorder, where Cu and Zn atoms are distributed randomly on the 2c and 2d Wyckoff positions. The ordering increases below this temperature and the perfect order is reached only at 0 K when the so-called equilibrium state is reached. However, this transition occurs only slowly with time and it is not possible to obtain perfectly ordered material. The degree of disorder often depends on the cooling rate of the sample after growth or after high-temperature treatment along with the cation composition in the material [30]. Many attempts have been made to correlate the degree of Cu-Zn disorder to the recombination processes in the bulk of CZTSe and CZTS, however, contradictory results have been obtained.

A few studies regarding pure selenide and sulfoselenide kesterites claim that ordering increases V_{OC} of solar cells. Nevertheless, in all cases, V_{OC} strictly follows the bandgap variations upon ordering. This means Cu-Zn disorder does not have a direct effect on the V_{OC} deficit and device performances [27,31]. Unlike what was believed before, Cu-Zn disorder is not directly responsible for tail-states either [32]. Among these studies, Rey *et al.* [4] proposed that $(2Cu_{Zn}^{-}+Sn_{Zn}^{2+})$ defect clusters have a significant impact on the band-edge energy and bandgap fluctuations. Timmo *et al.* [33] reported a V_{OC} improvement in CZTS monograins with the decrease in disorder, which was followed by a decrease in V_{OC} values for longer cooling times (up to 510 min). This reduction in V_{OC} is explained by the change in radiative recombination mechanism in the slowest cooled sample from band to tail to deep trap (~200 meV) related recombination. This recombination model is supported by the study of Bishop *et al.* [27] where the PL peak position of the slow-cooled sample showed a stronger blueshift (40 meV in comparison to 6 meV/decade) with increasing laser power. Both PL peaks were assigned to donor-acceptor pair recombinations. The more severe blueshift for the slow-cooled sample was explained by significant local potential fluctuations. The same group performed Hall measurements with the same CZTSe single crystals and obtained hole mobilities that were increased from 50 $cm^2/(V{\cdot}s)$ for quenched to 180 $cm^2/(V{\cdot}s)$ for slow-cooled crystals consistent with increasing crystalline order. Carrier concentrations on the other hand decreased from $3{\cdot}10^{18}/cm^3$ for quenched samples to $10^{16}/cm^3$ for slow-cooled crystals. The suggested reason is that in the quenched sample with high carrier concentration, band perturbations from charged defects are screened, while the slow-cooled sample still contains high defect concentrations but fewer free carriers.

In this work, we applied slow and rapid cooling to the CZTSe microcrystals annealed at high temperatures and report the influence of the degree of disorder on the defect structure and related radiative recombination processes studied by photoluminescence spectroscopy.

2. Experimental

CZTSe microcrystals were synthesized from high purity (99.999%) binaries CuSe, ZnSe, SnSe and elemental Se in an evacuated quartz ampoule at 740 °C using the liquid phase KI (potassium iodide) as a flux material. The temperature of the furnace was increased from room temperature (RT) to 740 °C within 5 h and then kept for 96 h at this temperature. After the synthesis, the ampoule was taken out of the furnace and cooled down to room temperature in air. The water-soluble KI was removed by washing with deionized water and the powder was then sieved into several granulometric fractions between 36 and 140 μm. To clean the crystal surfaces from secondary phases like Cu_xSe and $SnSe_2$, the powders were subjected to chemical etching for 30 min at 50 °C with a 10% aqueous solution of KCN (10 wt% KCN + 1 wt% KOH) in an ultrasonic bath. Etched powders were annealed in sealed quartz ampoules at 550 °C for 15 min and cooled at two different rates intending to achieve various degrees of disorder. The first sample was cooled from 550 °C to RT in ambient air within 5 min and the second sample was kept in the furnace for 300 min with the natural cooling rate of the furnace. The samples will be named accordingly as disordered (Dis-CZTSe) and ordered (Ord-CZTSe) CZTSe in the following sections.

The microstructure of CZTSe powder crystals was studied by a high-resolution scanning electron microscope (SEM) Zeiss Ultra 55. The surface composition was analyzed by energy dispersive X-ray spectroscopy (EDX) system Bruker Esprit 1.82, which is equipped with an EDX-Xflash 3001 detector. An accelerating voltage of 20 kV was applied. The measurement error for elemental analysis is about 0.5 at.%. RT Raman spectra were measured using μ-Raman spectrometer HORIBA LabRAM 800HR. Nd:YAG laser beam with a wavelength of 532 nm is used for the excitation and it was focused on the sample with an x50 objective. The scattered laser light is analyzed by using 1800 lines/mm grating monochromator and a Si CCD detector. For PL measurements, the samples were mounted on the cold finger of the closed-cycle helium cryostat (Janis CCS-150) and cooled down to 8 K. The temperature was adjusted up to RT via a temperature controller (LakeShore Model 335). The He-Cd laser with a wavelength of 441 nm was used for PL excitation. The power of the incident laser beam was altered via neutral density

filters between 0.77 and 37.1 mW. An optical chopper was used for modulating the laser light. The emitted light was conditioned using a cut-off low-pass filter and focused on the computer-controlled single grating (600 mm^{-1}) monochromator (f = 0.64 m) (Horiba Jobin Yvon FHR640). Luminescence was dispersed by the monochromator and detected by the Hamamatsu InGaAs photomultiplier tube. Stanford SR810 DSP lock-in amplifier was used for amplifying the PL signal.

3. Results and discussion

The elemental composition of microcrystals was determined from the surface of 8 different individual crystals for each sample by EDX measurements. The average atomic ratio of each element together with Cu/(Zn + Sn) and Zn/Sn ratios are presented in Table 1. According to the results, the composition does not vary with the change in the degree of disorder and both samples are Cu-poor, Zn and Sn stoichiometric. Fig. 1 shows the SEM image of Ord-CZTSe. The sample consists of mostly roundly shaped microcrystals with flat facets and smooth edges.

Raman spectroscopy was performed on the top surface of both microcrystalline samples to evaluate the effect of different cooling rates on the vibrational modes of molecules. Fig. 2 compares the normalized Raman spectra for Dis-CZTSe and Ord-CZTSe. The spectra were fitted with Lorentzian curves and the resulting peaks were attributed to the CZTSe kesterite phase [34,35]. We focused on the Raman modes with A symmetry. In Ord-CZTSe sample, these modes are labeled as A(1), A(2), and A(3). According to the mode symmetry analysis, these three Raman-active A modes in Dis-CZTSe sample become two Raman-active A_1 modes $A_1(1)$ and $A_1(2)$. The fitting results are given in Table 2. We also added data for ordered and disordered samples from Ref. [26] for comparison, where the disordered sample was annealed at 300 °C for 1 h and quenched, thereafter, the ordered sample has been treated further with the following annealing sequence: 150 °C for 2 h, 125 °C for 20 h, 100 °C for 20 h, 80 °C for 18 h. With the decrease in disorder, the linewidths (FHWM) for the main A symmetry modes narrowed in accordance with the change in the disorder. It is visible, that our microcrystalline powders show very similar Raman peaks, but there is a small deviation in values of peak positions E_{max} showing that our samples are less ordered and less disordered than the samples from Ref. [26]. Ordering also shifts the main peaks toward higher wavenumbers, which can be explained by the decrease in defect density, hence the increase in correlation length [26].

Temperature-dependent PL spectra of CZTSe microcrystals with different degrees of disorder are presented in Fig. 3. All spectra were fitted with a single asymmetric double sigmoidal function. The peak position of the low-temperature PL band shifted from 0.88 eV to 0.92 eV with the decrease in disorder. This behavior is in correlation with previous works [10,33]. The average depth of potential fluctuations γ was determined from the slope of the low energy side of the PL band as 28 and 24 meV for Dis-CZTSe and Ord-CZTSe, respectively, and indicates similar charged defect concentrations for both samples [10]. Electrostatic fluctuations are often formed in multinary compounds due to the high concentration of charged defects and a high degree of compensation. Since the amplitude of the fluctuations is only a weak function of temperature, it is determined at low temperatures, where the role of electron-phonon interactions on the shape of PL bands is very small [36].

The wide and asymmetric PL band in CZTSe is a typical indication of recombination involving valence and conduction band tails formed by

Table 1
EDX elemental composition of both Dis-CZTSe and Ord-CZTSe.

Sample	Cu (at %)	Zn (at %)	Sn (at %)	Se (at %)	Cu/(Zn + Sn)	Zn/Sn
Ord-/Dis-CZTSe	23.17	13.34	13.49	50.00	0.86	0.99

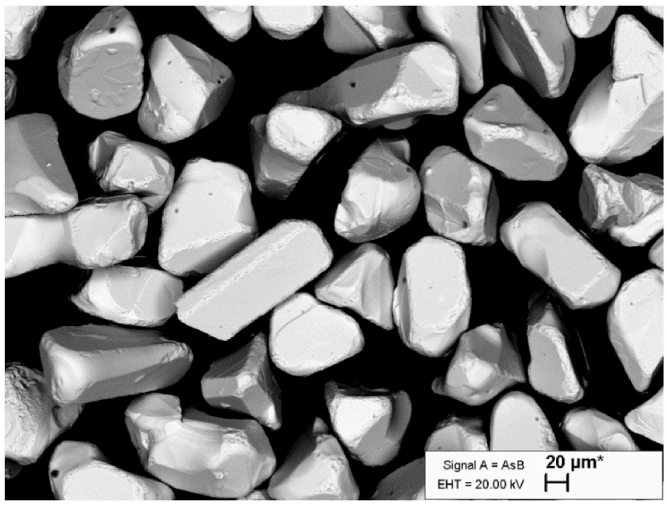

Fig. 1. Scanning electron microscope image of individual microcrystals of Ord-CZTSe sample. Crystals were selected from the fractions between 63 and 75 µm.

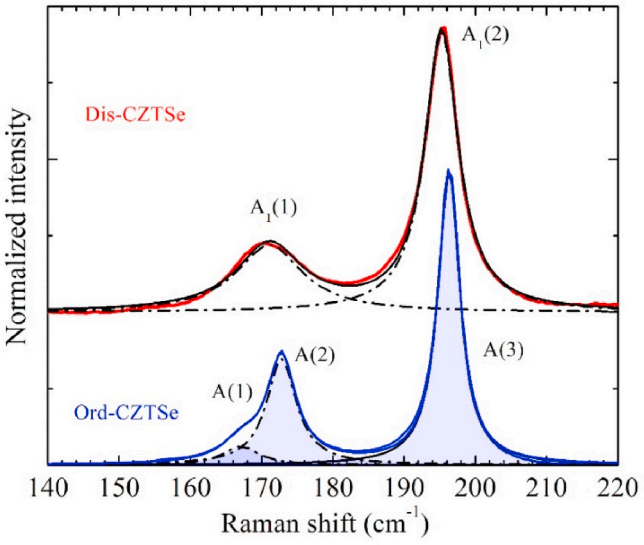

Fig. 2. Room temperature Raman spectra of disordered (Dis-CZTSe) and ordered (Ord-CZTSe) $Cu_2ZnSnSe_4$ microcrystals.

Table 2
Results of Raman spectra fitting for Dis-CZTSe and Ord-CZTSe. Data from Ref. [26] is also given for comparison.

Raman peak	$A_1(1)$		$A_1(2)$	
	E_{max} (cm^{-1})	FWHM (cm^{-1})	E_{max} (cm^{-1})	FWHM (cm^{-1})
Dis-CZTSe	**171.1**	**11.2**	**195.3**	**5.8**
Data from [26]	*170.6*	*10.8*	*194.6*	*5.7*

Raman peak	A(1)		A(2)		A(3)	
	E_{max} (cm^{-1})	FWHM (cm^{-1})	E_{max} (cm^{-1})	FWHM (cm^{-1})	E_{max} (cm^{-1})	FWHM (cm^{-1})
Ord-CZTSe	**167.1**	**6.0**	**172.8**	**5.0**	**196.3**	**3.8**
Data from [26]	*168.1*	*5.3*	*173.0*	*5.7*	*196.4*	*3.7*

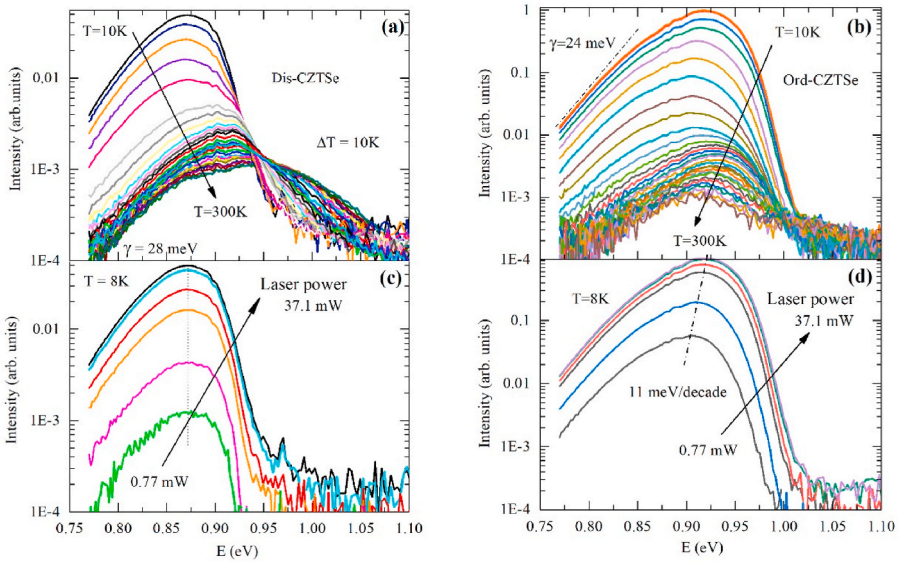

Fig. 3. Temperature dependence of PL spectra of **(a)** Dis-CZTSe **(b)** Ord-CZTSe. Excitation power dependence of PL spectra of **(c)** Dis-CZTSe **(d)** Ord-CZTSe. The dashed-dotted line presents the determination of γ in Fig. 3 (b).

spatial potential fluctuations in highly doped semiconductors [14, 37–39]. It was shown that the edge emission in highly doped and compensated semiconductors largely includes 3 typical emission bands: BT, BI and BB bands. The BT-band usually dominates at low temperatures while the BB-band becomes visible at high temperatures and high excitation intensities. The presence of the BI-band ("impurity" here is related to deep intrinsic acceptor defect) depends on the occurrence of a suitable defect level. At low temperatures, due to the potential fluctuations, the holes are mostly captured by deep valence band states within the fundamental energy gap. These deep band states form localized states for holes that look more like acceptor levels. Due to their small effective mass electrons typically do not form similar bound states near the conduction band edge. However, in some cases, the potential wells for electrons can be very deep and thus the tail-to-impurity (TI) and tail-to-tail (TT) recombination are possible [21]. For example, conduction band tail related recombination is possible if donor defects form clusters involving several defects. In this case potential wells, that are deep enough for electrons to be localized, are formed and due to the bending of the bands near a donor cluster, as the separation r between the donor cluster and the acceptor states decreases, the energy of acceptor states increases. At low temperatures, electrons are distributed in localized tail states. Since the holes cannot approach the donor wells too closely, electrons can only recombine with holes localized on distant acceptors, with a relatively low probability and lower energy. TI recombination can be compared to donor-acceptor pair recombination. It must be noted that TI recombination can give rise to two separate emission bands: a band originating from deeper wells referred to here as TI_2 and a band originating from shallower wells referred to as TI_1. The density of shallower wells is much larger than the density of deeper wells. Therefore, at very low temperatures TI_1 recombination dominates. When the temperature is increased, localized electrons from shallower wells are transferred into deeper wells and the peak position of the TI band is shifting toward lower energy due to TI_2 recombination. Further increase in temperature leads to a blueshift of the TI_2 band according to the formula [14]:

$$E_{max}^{TI} = E_g^0 - \gamma_e - E_a + 2\sqrt{kT\gamma_e} \quad (1)$$

where E_g^0 is the bandgap energy, γ_e is the average depth of potential fluctuations for electrons, E_a is the depth of the acceptor level and T is the temperature.

Dual redshift and blueshift behavior of the peak position below 100 K for both samples is consistent with the TI transition. The energy separation between deeper and shallower clusters is ~10 meV for Dis-CZTSe and ~20 meV for Ord-CZTSe sample, see Fig. 4. It should be noted that this behavior is only possible if the excitation level is weak enough. The redshift beginning from the lowest temperatures is due to the lowering

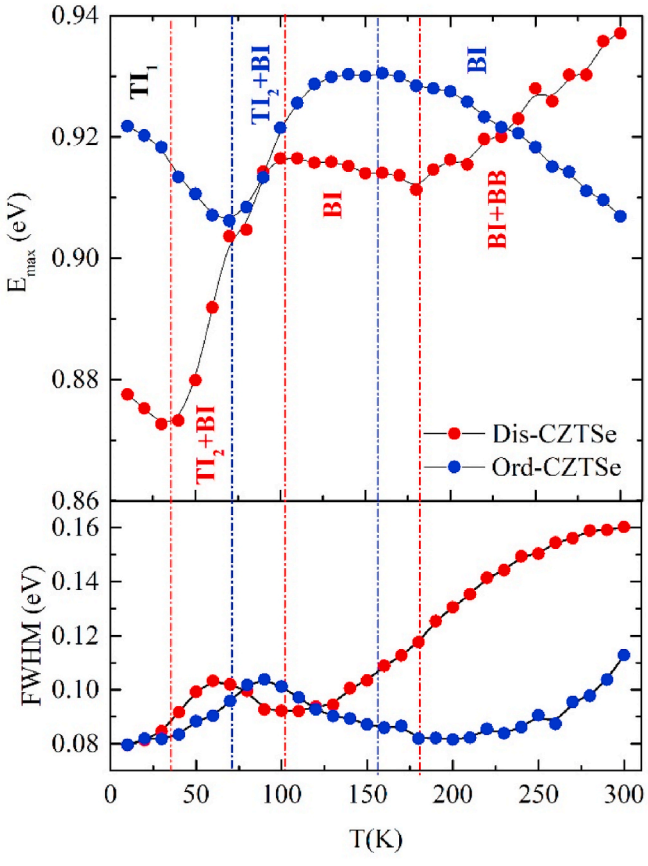

Fig. 4. Temperature dependence of the PL peak position (E_{max}) in comparison with the linewidth of the PL peak (FWHM) for Dis-CZTSe and Ord-CZTSe.

of electron quasi-Fermi level, i.e., due to the thermal liberation of electrons from the shallower donor wells and the following blueshift is due to the thermal emptying of deeper donor wells. At the same time, the donor cluster model with acceptors having different distances from the cluster means, that the intensity of this TI band has a maximum at temperatures T > 30–40K. According to Levanyuk and Osipov [14], the intensity of the TI band can be given as:

$$\varphi_{TI}(T) \propto exp\left[-\left(kTln\frac{N_C}{n} + \gamma_e \right)^{1/2} \left(4kT^{-1/2} + \gamma_e^{-1/2} \right) \right] \quad (2)$$

where γ_e is an average depth of potential fluctuations for electrons, n is the electron concentration, N_C is the density of conduction band states and T is the temperature. Analysis of this equation shows, that the intensity of the TI recombination for the donor cluster model is small at low temperatures and also at higher temperatures. The low-temperature quenching is related to the fact, that holes cannot approach donor clusters and the recombination probability for distant holes is exponentially small. We did not notice any intensity drop at lower temperatures in both samples. This means that this TI model with donor defect clusters seems not to be suitable in our case.

However, TI recombination with relatively deep potential wells for electrons can also be caused by different neutral defect clusters [16,20]. While some clusters like $(Cu_{Sn}^{-} + Sn_{Cu}^{+})$ create very deep potential wells for both electrons and holes, some of them like $(2V_{Cu}^{-} + Sn_{Zn}^{2+})$, $(V_{Zn}^{2-} + Sn_{Zn}^{2+})$, $(Zn_{Sn}^{2-} + Sn_{Zn}^{2+})$ and $(2Cu_{Zn}^{-} + Sn_{Zn}^{2+})$ induce mostly potential wells for electrons [16]. Deep potential wells for electrons caused by defect clusters are very similar to 3D quantum wells in different materials [25]. The initial redshift of the peak position with increasing temperature at very low temperatures is initiated by the redistribution of electrons from shallow wells into deeper ones. Accordingly, the rapid increase of the FWHM at $T \approx$ 20–60 K could represent a crossover from nonthermalized to thermalized energy distribution of localized electrons, see Fig. 4. But in our case, higher values of FWHM can also be caused by the overlapping of TI and BI PL bands in both of our samples. Above $T \approx$ 100 K, the usual BI recombination starts to dominate. While the resulting temperature dependence of the peak position at T < 100K is similar for both TI models, the temperature dependence of FWHM is different and favors the neutral defect cluster model [22].

With further increasing the temperature, deeper wells are also emptied and a transition from TI to BI recombination may occur. We have observed the transition from TI to BI in heavily doped $CuGaTe_2$ crystals, see Ref. [21]. BI recombination involves free electrons having energy close to the Fermi level with holes localized at acceptor defects. The average depth of potential fluctuations γ has to be smaller than the ionization energy of the acceptor state E_a so that the acceptor state does not overlap with the valence band tail. The temperature dependence of a BI-band position first suffers a redshift until it reaches the critical temperature and then shifts towards higher energies by an amount of γ. This doesn't completely apply to our situation because we suggest that the low-temperature region is dominated by both TI and BI transitions until BI transition prevails. Despite the similar behavior of TI and BI band positions in regard to increasing temperature, the presence of BI recombination is detectable by the laser power dependence of the PL spectrum. In the Dis-CZTSe sample, the band does not shift according to laser power variations, see Fig. 3. This behavior was associated with BI transition before in heavily doped $CuInTe_2$ crystals [40]. In the case of the Ord-CZTSe sample, a blueshift with the magnitude of 11 meV per decade with increasing laser power is detected, which is typical for TI recombination (see Fig. 5).

Finally, the BI recombination starts to dominate. It is known, that starting from T ≈ 100K the peak position of the BI-band follows the temperature dependence of the bandgap energy [14,15]. The temperature dependence of bandgap energy of CZTSe can be found in Ref. [41]. At very high-temperatures BI recombination will be transferred to BB recombination and the peak position of the PL band will shift toward higher energy. Temperature quenching of the PL of both samples shows clearly two separate processes, see Fig. 6 (a). Both processes were fitted by using the theoretical expression for discrete energy levels [42]:

$$\Phi(T) = \Phi_0 \,/\, \left[1 + A_1 T^{3/2} + A_2 T^{3/2}\, exp(-E_A \,/\, kT) \right] \quad (3)$$

where Φ is the integrated intensity of the PL band, A_1 and A_2 are the process rate parameters and E_A is the thermal activation energy. Unfortunately, we could not get a good fit for the Dis-CZTSe sample, because at higher temperatures the linear part of the relation is missing due to the coexistence of BI and BB emissions. The low-temperature quenching of the PL of the Ord-CZTSe sample with an activation energy of E_{A1} = 28 meV is related to the emptying of potential wells for electrons and the high-temperature quenching (E_{A2} = 85 meV) is caused by ionization of deep acceptor levels.

The excitation power dependence of the integrated PL band intensity Φ for both samples (see Fig. 6 (b)) shows a dependence, that can be described by the power law $\Phi \sim P^k$, where P is the excitation power and k is the exponent. The k-value, which is an indication of the type of recombination, was extracted from the linear fit of the plot and resulted in 0.8 for Ord-CZTSe and 0.9 for Dis-CZTSe. This is evidence that the recombination is defect related. However, at high excitation powers, the slope of the Ord-CZTSe sample is reduced, which can be ascribed to the saturation of the optical centers responsible for the PL or to the involuntary temperature increase at high excitation powers [15].

It seems, that both samples (Ord-CZTSe and Dis-CZTSe) show similar behavior, i.e. both have deep potential wells for electrons. At higher temperatures, the Ord-CZTSe sample does not have the transition from BI to BB recombination and the BI recombination dominates. This is an indication that the Ord-CZTSe sample has a deeper acceptor level. The temperature dependencies of E_{max} and FWHM indicate also, that the Ord-CZTSe sample has deeper wells for electrons, i.e. higher temperatures are needed to transform recombination from TI to BI. In accordance with the FWHM transformation, the minimum of E_{max} corresponds to a critical temperature value where redshift turns into blueshift. In theory, this value shifts towards higher temperatures with deeper potential wells for electrons. Although in our case the Ord-CZTSe sample has a smaller amplitude of potential fluctuations, it has deeper localized energy states for electrons. At the same time, in the Ord-CZTSe sample, the maximum shift of E_{max} is smaller than for the Dis-CZTSe sample. All these facts point to a different defect cluster in ordered and disordered samples.

As mentioned before, TI recombination in our samples favors the neutral defect cluster model. According to the theoretical calculations by Chen *et al.* [16], there are 4 possible candidates for self-compensated defect clusters which induce deep wells for electrons with a depth of around 100 meV: $(2V_{Cu}^{-} + Sn_{Zn}^{2+})$, $(V_{Zn}^{2-} + Sn_{Zn}^{2+})$, $(Zn_{Sn}^{2-} + Sn_{Zn}^{2+})$ and $(2Cu_{Zn}^{-} + Sn_{Zn}^{2+})$. All of them have the deep donor defect Sn_{Zn}^{2+} in common, which has the lowest formation energy among isolated donor defects together with shallow donor Zn_{Cu}^{+}. The $(2Cu_{Zn}^{-} + Sn_{Zn}^{2+})$ cluster has quite a low formation energy and induces an electron well of 120 meV, which is expected to form in Cu-poor, Zn-rich CZTSe [43]. Although all the candidates correlate with the energetic difference of PL bands, the conduction band shift is not accurate enough to explain the difference in depth of the quantum wells for electrons in our samples. The calculated activation energy E_{A2} = 85 meV in the Ord-CZTSe sample at high temperatures corresponds to the ionization of the acceptor defect Cu_{Zn}^{-}. Similar to 85 meV energy levels were obtained using both photoluminescence and admittance spectroscopy [9,44]. Acceptor defect Cu_{Zn}^{-} also has the lowest formation energy in CZTSe, which corresponds to a defect population of more than 10^{15} cm^{-3} [19]. We can assume that Cu_{Zn}^{-} is present in our samples independent of their degree of disorder.

Overall, we report that the change in disorder modified the defect structure but didn't have a significant effect on the average depth of potential fluctuations, the origin of the band tail states. The proposed

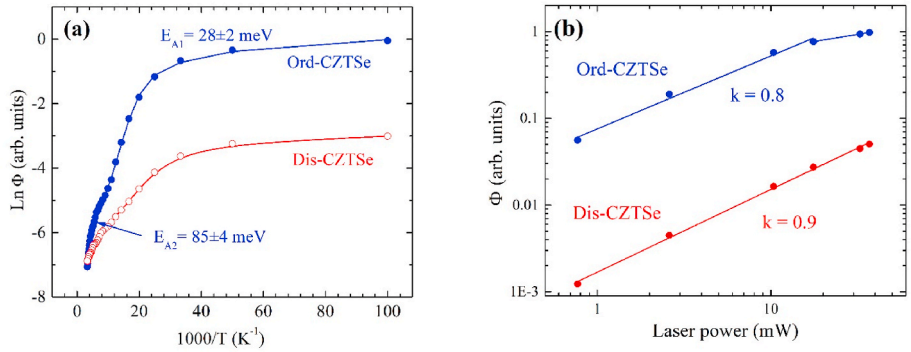

Fig. 5. (a) Arrhenius plot derived from the temperature dependence of PL spectra together with the obtained thermal activation energy values, E_A. Dots present the experimental data and solid lines present the fitting with the theoretical expression (3). The solid line for Dis-CZTSe is just a spline approximation and not a theoretical fitting result. **(b)** Laser power dependence of PL integrated intensity, Φ. Experimental data were fitted by a linear equation.

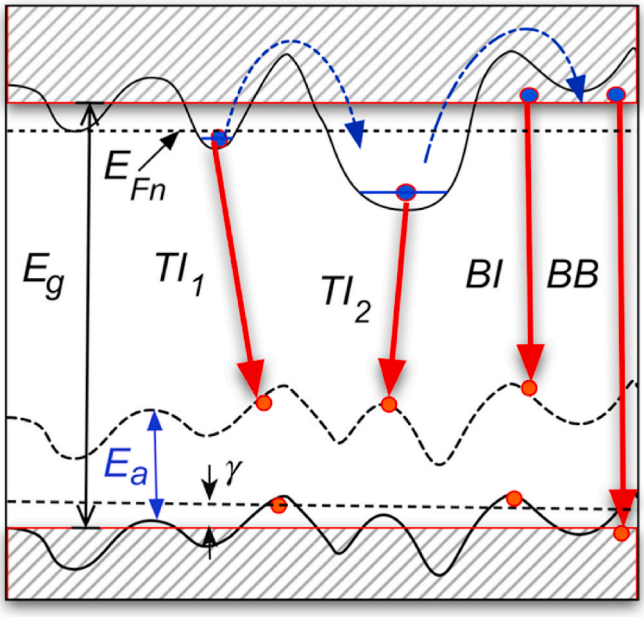

Fig. 6. Band structure and radiative recombination channels in CZTSe microcrystals showing fluctuating band edges and localized states for both electrons and holes.

recombination model for the studied microcrystals is presented in Fig. 6. At low temperatures, the dominating recombination mechanism occurs between electrons and holes in the potential well originating from a neutral defect cluster, where in Ord-CZTSe we observe deeper wells for electrons. When the temperature is high enough, the thermalization of localized electrons allows BI recombination to dominate. Due to the deeper acceptor level in Ord-CZTSe, the transition from BI to BB recombination does not take place. Considering the bandgap variation resulting from the change in disorder, the bandgap shift induced by neutral defect clusters in CZTSe adds up to our PL peak positions and calculated activation energies.

4. Conclusions

We present a PL study of CZTSe microcrystals with different degrees of disorder. The emission bands were located at 0.88 and 0.92 eV for Dis-CZTSe and Ord-CZTSe, respectively. The PL bands were attributed to TI and BI transitions coexisting at low temperatures, whereas at higher temperatures BI transition prevails and finally transforms to BB transition. In both samples, we detected localized electron states situating around 100 meV below the conduction band. The temperature dependencies of E_{max} and FWHM indicate that the Ord-CTZSe has deeper wells for electrons, where electrons redistribute from shallow into deeper wells with increasing temperature. The dominating recombination mechanism at low temperatures points to a neutral defect cluster involving Sn_{Zn}^{2+} donor defect and different depth of acceptor levels for each sample. The average depth of potential fluctuations γ in the valence band edge was found as 28 and 24 meV for Dis-CZTSe and Ord-CZTSe, respectively, indicating similar charged defect concentrations for both samples.

CRediT authorship contribution statement

İ. Mengü: Conceptualization, Data curation, Methodology, Formal analysis, Writing – original draft, Writing – review & editing. **J. Krustok:** Conceptualization, Data curation, Methodology, Supervision, Formal analysis, Writing – original draft, Writing – review & editing. **R. Kaupmees:** Methodology. **V. Mikli:** Methodology. **M. Kauk-Kuusik:** Writing – review & editing, Supervision, Resources, Funding acquisition, Formal analysis, Conceptualization. **M. Grossberg-Kuusk:** Writing – review & editing, Writing – original draft, Supervision, Resources, Funding acquisition, Formal analysis, Data curation, Conceptualization.

Declaration of competing interest

The authors declare that they have no known competing financial interests or personal relationships that could have appeared to influence the work reported in this paper.

Data availability

Data will be made available on request.

Acknowledgements

This work was supported by ERDF projects TK141 and "NAMUR+ (2020.4.01.16-0123)" and by the Estonian Research Council grant PRG1023.

References

[1] M. Grossberg, J. Krustok, C.J. Hages, D.M. Bishop, O. Gunawan, R. Scheer, S. M. Lyam, H. Hempel, S. Levcenco, T. Unold, The electrical and optical properties of kesterites, J. Phys.: Energy 1 (2019), 044002, https://doi.org/10.1088/2515-7655/ab29a0.

[2] M. Sahu, V.R. Minnam Reddy, C. Park, P. Sharma, Review article on the lattice defect and interface loss mechanisms in kesterite materials and their impact on solar cell performance, Sol. Energy 230 (2021) 13–58, https://doi.org/10.1016/j.solener.2021.10.005.

[3] J. Li, Y. Huang, J. Huang, G. Liang, Y. Zhang, G. Rey, F. Guo, Z. Su, H. Zhu, L. Cai, K. Sun, Y. Sun, F. Liu, S. Chen, X. Hao, Y. Mai, M.A. Green, Defect control for 12.5% efficiency $Cu_2ZnSnSe_4$ kesterite thin-film solar cells by engineering of local chemical environment, Adv. Mater. 32 (2020), 2005268, https://doi.org/10.1002/adma.202005268.

[4] G. Rey, G. Larramona, S. Bourdais, C. Choné, B. Delatouche, A. Jacob, G. Dennler, S. Siebentritt, On the origin of band-tails in kesterite, Sol. Energy Mater. Sol. Cell. 179 (2018) 142–151, https://doi.org/10.1016/j.solmat.2017.11.005.

[5] S. Schorr, G. Gurieva, M. Guc, M. Dimitrievska, A. Pérez-Rodríguez, V. Izquierdo-Roca, C.S. Schnohr, J. Kim, W. Jo, J.M. Merino, Point defects, compositional fluctuations, and secondary phases in non-stoichiometric kesterites, JPhys Energy 2 (2020), 012002, https://doi.org/10.1088/2515-7655/ab4a25.

[6] S. Oueslati, G. Brammertz, M. Buffière, C. Köble, T. Oualid, M. Meuris, J. Poortmans, Photoluminescence study and observation of unusual optical transitions in $Cu_2ZnSnSe_4$/CdS/ZnO solar cells, Sol. Energy Mater. Sol. Cell. 134 (2015) 340–345, https://doi.org/10.1016/j.solmat.2014.10.041.

[7] M.V. Yakushev, J. Márquez-Prieto, I. Forbes, P.R. Edwards, V.D. Zhivulko, A. V. Mudryi, J. Krustok, R.W. Martin, Radiative recombination in $Cu_2ZnSnSe_4$ thin films with Cu deficiency and Zn excess, J. Phys. D Appl. Phys. 48 (2015), 475109, https://doi.org/10.1088/0022-3727/48/47/475109.

[8] J. Márquez-Prieto, M.V. Yakushev, I. Forbes, J. Krustok, P.R. Edwards, V. D. Zhivulko, O.M. Borodavchenko, A.V. Mudryi, M. Dimitrievska, V. Izquierdo-Roca, N.M. Pearsall, R.W. Martin, Impact of the selenisation temperature on the structural and optical properties of CZTSe absorbers, Sol. Energy Mater. Sol. Cell. 152 (2016) 42–50, https://doi.org/10.1016/j.solmat.2016.03.018.

[9] M.V. Yakushev, M.A. Sulimov, J. Márquez-Prieto, I. Forbes, J. Krustok, P. R. Edwards, V.D. Zhivulko, O.M. Borodavchenko, A.V. Mudryi, R.W. Martin, Influence of the copper content on the optical properties of CZTSe thin films, Sol. Energy Mater. Sol. Cell. 168 (2017) 69–77, https://doi.org/10.1016/j.solmat.2017.04.022.

[10] M. Grossberg, J. Krustok, J. Raudoja, K. Timmo, M. Altosaar, T. Raadik, Photoluminescence and Raman study of $Cu_2ZnSn(Se_xS_{1-x})_4$ monograins for photovoltaic applications, Thin Solid Films 519 (2011) 7403–7406, https://doi.org/10.1016/j.tsf.2010.12.099.

[11] M. Grossberg, J. Krustok, K. Timmo, M. Altosaar, Radiative recombination in $Cu_2ZnSnSe_4$ monograins studied by photoluminescence spectroscopy, Thin Solid Films 517 (2009) 2489–2492, https://doi.org/10.1016/j.tsf.2008.11.024.

[12] F. Luckert, D.I. Hamilton, M.V. Yakushev, N.S. Beattie, G. Zoppi, M. Moynihan, I. Forbes, A.V. Karotki, A.V. Mudryi, M. Grossberg, J. Krustok, R.W. Martin, Optical properties of high quality $Cu_2ZnSnSe_4$ thin films, Appl. Phys. Lett. 99 (2011), 062104, https://doi.org/10.1063/1.3624827.

[13] M.V. Yakushev, I. Forbes, A.V. Mudryi, M. Grossberg, J. Krustok, N.S. Beattie, M. Moynihan, A. Rockett, R.W. Martin, Optical spectroscopy studies of $Cu_2ZnSnSe_4$ thin films, Thin Solid Films 582 (2015) 154–157, https://doi.org/10.1016/j.tsf.2014.09.010.

[14] A.P. Levanyuk, V.V. Osipov, Edge luminescence of direct-gap semiconductors, Sov. Phys. Usp. 24 (3) (1981) 187–215, https://doi.org/10.1070/PU1981v024n03ABEH004770.

[15] J.P. Teixeira, R.A. Sousa, M.G. Sousa, A.F. Da Cunha, P.A. Fernandes, P.M. P. Salomé, J.P. Leitão, Radiative transitions in highly doped and compensated chalcopyrites and kesterites: the case of Cu_2ZnSnS_4, Phys. Rev. B Condens. Matter 90 (2014), 235202, https://doi.org/10.1103/PhysRevB.90.235202.

[16] S. Chen, A. Walsh, X.G. Gong, S.H. Wei, Classification of lattice defects in the kesterite Cu_2ZnSnS_4 and $Cu_2ZnSnSe_4$ earth-abundant solar cell absorbers, Adv. Mater. 25 (2013) 1522–1539, https://doi.org/10.1002/adma.201203146.

[17] I.S. Shlimak, V.P. Dobrego, The influence of local potential fluctuations on the low-temperature radiative recombination of compensated gernianium, Phys. Status Solidi 33 (1969) 805, https://doi.org/10.1002/pssb.19690330234.

[18] B.I. Shklovskii, A.L. Efros, Electronic properties of doped semiconductors, Springer Ser. Solid-state Sci. 45, doi:10.1007/978-3-662-02403-4.

[19] S. Chen, L.W. Wang, A. Walsh, X.G. Gong, S.H. Wei, Abundance of $Cu_{Zn} + Sn_{Zn}$ and $2Cu_{Zn} + Sn_{Zn}$ defect clusters in kesterite solar cells, Appl. Phys. Lett. 101 (2012), 223901, https://doi.org/10.1063/1.4768215.

[20] M. Grossberg, T. Raadik, J. Raudoja, J. Krustok, Photoluminescence study of defect clusters in Cu_2ZnSnS_4 polycrystals, Curr. Appl. Phys. 14 (2014) 447–450, https://doi.org/10.1016/j.cap.2013.12.029.

[21] A. Jagomägi, J. Krustok, M. Grossberg, M. Danilson, J. Raudoja, Deep defect related photoluminescence in heavily doped $CuGaTe_2$ crystals, Physica Status Solidi (A) Appl. Mater. Sci. 203 (2006) 949–955, https://doi.org/10.1002/pssa.200521118.

[22] S.A. Lourenço, I.F.L. Dias, J.L. Duarte, E. Laureto, V.M. Aquino, J.C. Harmand, Temperature-Dependent Photoluminescence Spectra of GaAsSb/AlGaAs and GaAsSbN/GaAs Single Quantum Wells under Different Excitation Intensities, Braz. J. Phys. 37 (2007) 4, https://doi.org/10.1590/S0103-97332007000800004.

[23] J. Krustok, T. Raadik, R. Kaupmees, M. Grossberg, M. Kauk-Kuusik, K. Timmo, A. Mere, Observation of band gap fluctuations and carrier localization in $Cu_2CdGeSe_4$, J. Phys. D Appl. Phys. 52 (2019), 285102, https://doi.org/10.1088/1361-6463/ab1afd.

[24] B.W. Zhang, D. Fang, X. Fang, H. Bin Zhao, D.K. Wang, J.H. Li, X.H. Wang, D. B. Wang, InAs/InAsSb type-II superlattice with near room-temperature long-wave emission through interface engineering, Rare Met. 41 (2022) 982–991, https://doi.org/10.1007/s12598-021-01833-x.

[25] H. Wang, Z. Ji, S. Qu, G. Wang, Y. Jiang, B. Liu, X. Xu, H. Mino, Influence of excitation power and temperature on photoluminescence in InGaN/GaN multiple quantum wells, Opt Express 20 (2012) 3932–3940, https://doi.org/10.1364/OE.20.003932.

[26] G. Rey, A. Redinger, J. Sendler, T.P. Weiss, M. Thevenin, M. Guennou, B. el Adib, S. Siebentritt, The band gap of $Cu_2ZnSnSe_4$: effect of order-disorder, Appl. Phys. Lett. 105 (2014), 112106, https://doi.org/10.1063/1.4896315.

[27] D.M. Bishop, B. McCandless, T. Gershon, M.A. Lloyd, R. Haight, R. Birkmire, Modification of defects and potential fluctuations in slow-cooled and quenched $Cu_2ZnSnSe_4$ single crystals, J. Appl. Phys. 121 (2017), 065704, https://doi.org/10.1063/1.4975483.

[28] R.D. Shannon, Revised effective ionic radii and systematic studies of interatomie distances in halides and chaleogenides, Acta Crystallogr. A32 (1976) 751–767, https://doi.org/10.1107/S0567739476001551.

[29] S. Chen, J.H. Yang, X.G. Gong, A. Walsh, S.H. Wei, Intrinsic point defects and complexes in the quaternary kesterite semiconductor Cu_2ZnSnS_4, Phys. Rev. B Condens. Matter 81 (2010), 245204, https://doi.org/10.1103/PhysRevB.81.245204.

[30] K. Rudisch, A. Davydova, C. Platzer-Björkman, J. Scragg, The effect of stoichiometry on Cu-Zn ordering kinetics in Cu_2ZnSnS_4 thin films, J. Appl. Phys. 123 (2018), 161558, https://doi.org/10.1063/1.5010081.

[31] S. Bourdais, C. Choné, B. Delatouche, A. Jacob, G. Larramona, C. Moisan, A. Lafond, F. Donatini, G. Rey, S. Siebentritt, A. Walsh, G. Dennler, Is the Cu/Zn disorder the main culprit for the voltage deficit in kesterite solar cells? Adv. Energy Mater. 6 (2016), 1502276 https://doi.org/10.1002/aenm.201502276.

[32] S. Ma, H. Li, J. Hong, H. Wang, X. Lu, Y. Chen, L. Sun, F. Yue, J.W. Tomm, J. Chu, S. Chen, Origin of band-tail and deep-donor states in Cu_2ZnSnS_4 solar cells and their suppression through Sn-poor composition, J. Phys. Chem. Lett. 10 (2019) 7929–7936, https://doi.org/10.1021/acs.jpclett.9b03227.

[33] K. Timmo, M. Kauk-Kuusik, M. Pilvet, T. Raadik, M. Altosaar, M. Danilson, M. Grossberg, J. Raudoja, K. Ernits, Influence of order-disorder in Cu_2ZnSnS_4 powders on the performance of monograin layer solar cells, Thin Solid Films 633 (2017) 122–126, https://doi.org/10.1016/j.tsf.2016.10.017.

[34] M. Guc, S. Levcenko, V. Izquierdo-Roca, X. Fontané, E. Arushanov, A. Pérez-Rodríguez, Polarized Raman scattering analysis of $Cu_2ZnSnSe_4$ and $Cu_2ZnGeSe_4$ single crystals, J. Appl. Phys. 114 (2013), 193514, https://doi.org/10.1063/1.4830028.

[35] M. Dimitrievska, A. Fairbrother, E. Saucedo, A. Pérez-Rodríguez, V. Izquierdo-Roca, Influence of compositionally induced defects on the vibrational properties of device grade $Cu_2ZnSnSe_4$ absorbers for kesterite based solar cells, Appl. Phys. Lett. 106 (2015), 073903, https://doi.org/10.1063/1.4913262.

[36] S. Siebentritt, N. Papathanasiou, M.C. Lux-Steiner, Potential fluctuations in compensated chalcopyrites, Phys. B Condens. Matter 376–377 (2006) 831–833, https://doi.org/10.1016/j.physb.2005.12.208.

[37] J. Krustok, H. Collan, M.V. Yakushev, K. Hjelt, The role of spatial potential fluctuations in the shape of the PL bands of multinary semiconductor compounds, Phys. Scripta T79 (1999) 179–182, https://doi.org/10.1238/Physica.Topical.079a00179.

[38] J. Krustok, J. Raudoja, M. Yakushev, R.D. Pilkington, H. Collan, On the shape of the close-to-band-edge photoluminescent emission spectrum in compensated $CuGaSe_2$, Phys. Status Solidi 173 (1999) 483–490, https://doi.org/10.1002/(SICI)1521-396X(199906)173:2<483::AID-PSSA483>3.0.CO;2-A.

[39] I. Dirnstorfer, M.T. Wagner, D.M. Hofmann, M.D. Lampert, F. Karg, B.K. Meyer, Characterization of CuIn(Ga)Se_2 thin films III. In-rich layers, Physica Status Solidi A Appl. Res. 168 (1998) 163–175, https://doi.org/10.1002/(SICI)1521-396X(199807)168:1<163::AID-PSSA163>3.0.CO;2-T.

[40] A. Jagomägi, J. Krustok, J. Raudoja, M. Grossberg, M. Danilson, M. Yakushev, Photoluminescence studies of heavily doped $CuInTe_2$ crystals, Phys. B Condens. Matter 337 (2003) 369–374, https://doi.org/10.1016/S0921-4526(03)00429-0.

[41] S.G. Choi, T.J. Kim, S.Y. Hwang, J. Li, C. Persson, Y.D. Kim, S.H. Wei, I.L. Repins, Temperature dependent band-gap energy for $Cu_2ZnSnSe_4$: a spectroscopic ellipsometric study, Sol. Energy Mater. Sol. Cell. 130 (2014) 375–379, https://doi.org/10.1016/j.solmat.2014.07.039.

[42] J. Krustok, H. Collan, K. Hjelt, Does the low-temperature Arrhenius plot of the photoluminescence intensity in CdTe point towards an erroneous activation energy? J. Appl. Phys. 81 (1997) 1442–1445, https://doi.org/10.1063/1.363903.

[43] G. Gurieva, L.E. Valle Rios, A. Franz, P. Whitfield, S. Schorr, Intrinsic point defects in off-stoichiometric $Cu_2ZnSnSe_4$: a neutron diffraction study, J. Appl. Phys. 123 (2018), 161519, https://doi.org/10.1063/1.4997402.

[44] E. Kask, M. Grossberg, R. Josepson, P. Salu, K. Timmo, J. Krustok, Defect studies in $Cu_2ZnSnSe_4$ and $Cu_2ZnSn(Se_{0.75}S_{0.25})_4$ by admittance and photoluminescence spectroscopy, Mater. Sci. Semicond. Process. 16 (2013) 992–996, https://doi.org/10.1016/j.mssp.2013.02.009.